

# Light-Induced Polymer Response through Thermoplasmonics Transduction in Highly Monodisperse Core-Shell-Brush Nanosystems

María Jazmín Penelas,<sup>§</sup> Cintia Belén Contreras,<sup>\*,§</sup> Paula C. Angelomé, Alejandro Wolosiuk, Omar Azzaroni, and Galo J.A.A. Soler-Illia<sup>\*</sup>



Cite This: *Langmuir* 2020, 36, 1965–1974



Read Online

ACCESS |



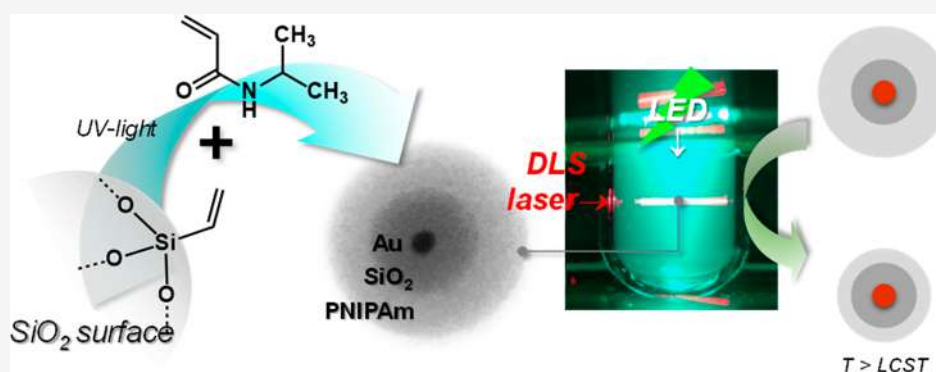
Metrics & More



Article Recommendations



Supporting Information



**ABSTRACT:** Smart nanosystems that transduce external stimuli to physical changes are an inspiring challenge in current materials chemistry. Hybrid organic–inorganic materials attract great attention due to the combination of building blocks responsive to specific external solicitations. In this work, we present a sequential method for obtaining an integrated core-shell-brush nanosystem that transduces light irradiation into a particle size change through a thermoplasmonic effect. We first synthesize hybrid monodisperse systems made up of functionalized silica colloids covered with controllable thermoresponsive poly(*N*-isopropylacrylamide), PNIPAm, brushes, produced through radical photopolymerization. This methodology was successfully transferred to Au@SiO<sub>2</sub> nanoparticles, leading to a core-shell-brush architecture, in which the Au core acts as a nanosource of heat; the silica layer, in turn, adapts the metal and polymer interfacial chemistries and can also host a fluorescent dye for bioimaging. Upon green LED irradiation, a light-to-heat conversion process leads to the shrinkage of the external polymer layer, as proven by *in situ* DLS. Our results demonstrate that modular hybrid nanosystems can be designed and produced with photothermo-physical transduction. These remote-controlled nanosystems present prospective applications in smart carriers, responsive bioscaffolds, or soft robotics.

## INTRODUCTION

The field of materials with stimuli-responsive properties has experienced an impressive growth during the last years, due to their potential high impact in fields such as drug delivery, energy storage, bioelectronics, wearable sensors, biomaterials, medical imaging, tissue regeneration, catalysis, or soft robotics.<sup>1–4</sup> The basic concept of stimuli-responsive materials, also known as “smart”, “intelligent”, or “adaptive” materials, implies control and exploitation of relatively large and abrupt physical or chemical changes as responses to external stimuli,<sup>5–7</sup> such as temperature, pH, redox potential, light, ionic strength, and magnetic fields.<sup>8–15</sup>

The design of these platforms takes advantage of a well-established “library” of functionalized nanomaterials combining different building blocks such as polymeric liposomes, dendrimers, self-assembled objects, inorganic nanoparticles,

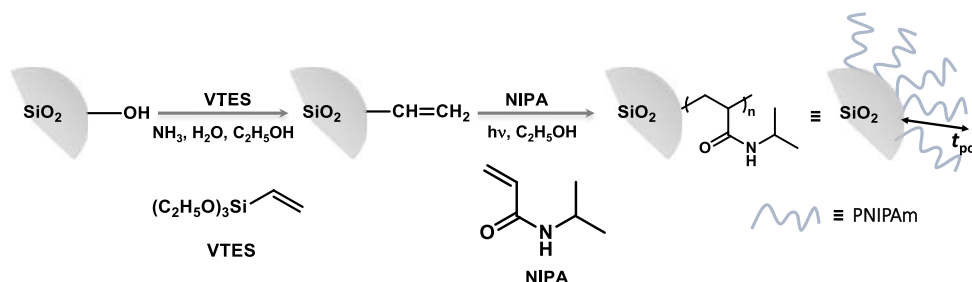
metal nanoparticles, carbon nanotubes, and mesoporous silica.<sup>16–20</sup> These systems can be tailor-made with a large variety of architectures and in diverse physical forms, adjustable to the requirements of their final application, by selection of the strategies of synthesis and functionalization.

Many functional molecules, polymers, or nanostructures have been developed that have paved the way to a new class of stimuli-sensitive materials. In particular, light triggers permit a facile control of the stimulus, through the arbitrary choices of wavelength, irradiation time, and localization.<sup>21,22</sup> Metal

**Received:** September 30, 2019

**Revised:** February 6, 2020

**Published:** February 6, 2020

Scheme 1. Simplified Description of Synthetic Steps Used in Preparation of (SiO<sub>2</sub>-V)-g-PNIPAm NPs

nanoparticles are attractive due to their enormous variety of compositions, sizes, and shapes that give rise to distinctive optical and catalytic properties.<sup>23,24</sup> Gold nanoparticles (Au NPs) show great advantages in the biomedical field because of their biocompatibility and noncytotoxicity.<sup>25–27</sup> The exposure of Au nanocarriers to an external light source leads to strong absorption and/or scattering at the Localized Surface Plasmon Resonance (LSPR), which leads to heat dissipation into the particle surroundings. This thermoplasmonic effect can be purposefully directed to therapeutic and diagnostic applications, through the exploitation of local light-induced heating.<sup>7,28–30</sup>

Polymers with a lower critical solution temperature (LCST) have been largely explored as building blocks that introduce temperature responsiveness into smart systems. Poly(*N*-isopropylacrylamide), PNIPAm, is a well-established temperature-responsive material used in drug delivery systems, human gene delivery vectors, biocatalysts, super absorbents, and devices for separation and purification of metal ions and biomolecules.<sup>31–34</sup> PNIPAm undergoes a phase transition from a hydrophobic to a hydrophilic state when the external temperature is below the LCST of about 32 °C in aqueous solution, a temperature range that depends on the polymer length and cross-linking.<sup>13</sup> Recently, Wu and co-workers combined Au and PNIPAm microgels producing a thermosensitive yolk–shell system that proved to be an effective light-triggered catalyst for the reduction of 4-nitrophenol and nitrobenzene in aqueous solution.<sup>35</sup> Shen and co-workers fabricated a yolk–shell thermosensitive nanoparticle using PNIPAm microgel and the silica-etching method. In this case, the nanoparticles were developed using Fe<sub>3</sub>O<sub>4</sub> nanoparticles as photothermal cores and applied as a remote-controlled targeting drug delivery platform for multimodal imaging and combined therapy of cancer.<sup>36</sup>

In addition, the development of oxide shells on metallic nanoparticles allows the combination and integration of the plasmonic effects in a single core-shell nanosystem. Silica is a useful platform due to its optical transparency, colloidal stability, biocompatibility, and versatile surface modification.<sup>37,38</sup> Core-shell Au@SiO<sub>2</sub> nanoparticles<sup>30</sup> are efficient to prevent Au NPs from aggregation and deformation, while permitting access to the extensive silica surface functionalization chemistry.<sup>39–42</sup> In this context, Tian and collaborators reported a strategy to fabricate core–satellite multicomponent nanostructures, MNP@SiO<sub>2</sub>–PNIPAm–Au, with tunable interparticle distances and catalysis properties by the combination of surface-initiated reversible addition–fragmentation chain transfer (SI-RAFT) polymerization and self-assembly.<sup>43</sup> In an other report, Wang and co-workers synthesized near-infrared light-responsive plasmonic core-shell thermosensitive ionic microgels based on Au nanorods coated with microgel

shells of ionic liquids.<sup>44</sup> In both reports, authors used a SiO<sub>2</sub> shell on the metallic core surface in order to access the extended silica surface functionalization. More recently, Villaverde and colleagues reported the synthesis of a core–multishell gold nanorods, coated with mesoporous silica and further covered with a thermosensitive polymer, which is vectorized for selective internalization in melanoma cells, leading to on-demand release of cytotoxic compounds in response to near-IR irradiation.<sup>45</sup>

In this work, we present a reproducible and simple one-pot sequential method to create core-shell-brush nanosystems with light-induced size change. The methodology is based on controlling the modification of silica surfaces through a radical photopolymerization procedure, which permits the synthesis of hybrid nanoparticles containing PNIPAm brushes. This procedure can be applied to either monodisperse silica or plasmonic Au@SiO<sub>2</sub> nanoparticles to obtain well-dispersed colloids with controllable metallic core and shell sizes, and tunable thickness polymer coatings. We demonstrate that these core-shell-brush nanosystems present a transduction from light to heat that impacts the shrinkage of the polymeric shell, leading to a remote-controlled light-induced shrinkable nanosystem. The obtained results have practical implications in smart carriers or soft robotics. Finally, to the best of our knowledge, we report for the first time a new methodology to study *in situ* the effects of irradiation on the physical response of these systems and thus to directly witness the remote control of nanoparticle response.

## ■ MATERIALS AND METHODS

Tetraethylorthosilicate (98%, TEOS), HAuCl<sub>4</sub>·3H<sub>2</sub>O, sodium citrate, polyvinylpyrrolidone (PVP, MW = 10 kDa), vinyltriethoxysilane (97%, VTES), *N*-isopropylacrylamide (97%, NIPA), 2,2-dimethoxy-2-phenylacetophenone (99%, DMPA), benzophenone (99%, BP), and Ru(bpy)<sub>3</sub>Cl<sub>2</sub> were purchased from Sigma-Aldrich; concentrated aqueous ammonia and absolute ethanol, were obtained from Biopack; toluene and methanol were purchased from Merck. All chemicals were used as received. Water used was deionized (18 MΩ·cm) and filtered prior to solution preparation.

Core-shell-brush hybrid nanosystems were prepared by combining three building blocks, a gold core, silica shell, and a brush of poly(*N*-isopropylacrylamide), PNIPAm. Surface modification of core-shell NPs with PNIPAm brushes was performed using a photoinitiated free radical graft polymerization. This included these two stages:

- 1 Optimization of the synthesis conditions for PNIPAm grafting carried out using dense spherical silica nanoparticles (SiO<sub>2</sub> NPs), obtained from controlled growth from Si alkoxide precursor (TEOS) in aqueous ethanol, using ammonia solution as the catalyst.
- 2 Synthesis of core-shell Au@SiO<sub>2</sub> NPs and then, PNIPAm grafted on the Au@SiO<sub>2</sub> NPs surface using the previously optimized conditions.

Table 1. Evaluated conditions for PNIPAm photografting on SiO<sub>2</sub> NPs optimization<sup>a</sup>

Sample	C <sub>NP</sub> (%m/V)	Molar ratio N/VTES	Type of initiator (i)	% Molar ratio i/N	D <sub>i</sub> mean (nm)	PDI mean	t <sub>pol</sub> mean ± SD (nm)
SiO <sub>2</sub> -V					158	0.054	
a <sub>B</sub>	0.25	40	BP	1	172	0.056	14 ± 4
a <sub>B10</sub>	0.25	40	BP	10	164	0.087	6 ± 3
a <sub>D</sub>	0.25	40	DMPA	1	177	0.072	19 ± 3
C <sub>B</sub>	0.5	10	BP	1	163	0.073	5 ± 3
B <sub>B</sub>	0.5	20	BP	1	168	0.052	10 ± 4
A <sub>B</sub>	0.5	40	BP	1	179	0.051	21 ± 5
A <sub>D</sub>	0.5	40	DMPA	1	188	0.079	30 ± 5

<sup>a</sup>Final concentration of SiO<sub>2</sub> NPs in the reaction suspension (C<sub>NP</sub>), molar ratio between NIPA and organosilane (N/VTES), type of initiator (i) and molar ratio of initiator with respect to the monomer (i/N).

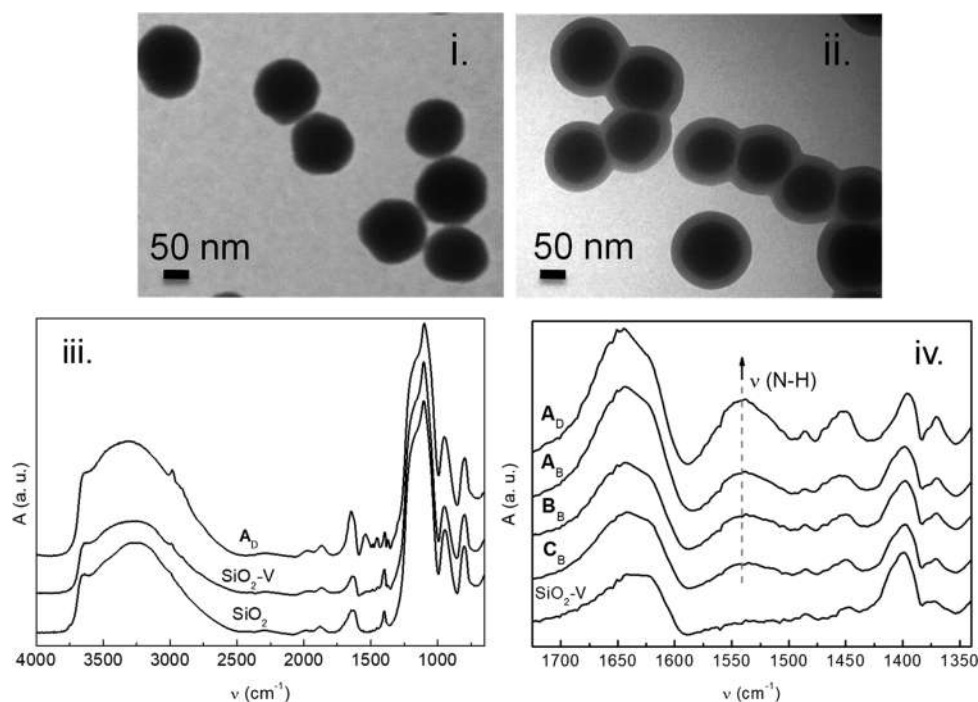


Figure 1. TEM images of NPs, (i) SiO<sub>2</sub>, and (ii) (SiO<sub>2</sub>-V)-g-PNIPAm. DRIFTS spectra of different NPs, SiO<sub>2</sub>, VTES functionalized and grafted with PNIPAm brushes (iii) and a zoom in PNIPAm signals region for different synthesis conditions of the core-brush NPs.

The experimental details regarding the nanoparticle preparation and the characterization techniques used are reported in the SI.

We should note that in the present work, for simplicity of expression, the term “polymer brush” is used as a synonym of the terms “tethered polymer chains” or “end-grafted polymers”. Strictly speaking, the term “polymer brush” should be associated with a layer of densely grafted polymer chains whose behavior is dictated by strong interactions between those chains.<sup>46–49</sup>

## RESULTS AND DISCUSSION

**Optimization of PNIPAm Photografting on SiO<sub>2</sub> NPs Surface.** The optimization of the synthesis conditions for PNIPAm grafting on the silica surface was carried out on dense SiO<sub>2</sub> NPs obtained by the Stöber method.<sup>50,51</sup> The molar concentrations of TEOS, NH<sub>3</sub>, and H<sub>2</sub>O used in synthesis were 0.17, 0.75, and 2 M, respectively, leading to highly monodisperse NPs of around 100 nm in diameter.

Surface modification of SiO<sub>2</sub> NPs with PNIPAm was performed using a photoinitiated free radical graft polymerization, by a two-stage process. Scheme 1 presents a simplified description of the PNIPAm grafting on SiO<sub>2</sub> NPs. In the first step, SiO<sub>2</sub> NPs were surface functionalized by a “one-pot”

reaction, with the addition of vinyltriethoxysilane (VTES) directly into the alcohol of the Stöber synthesis, resulting in vinyl modified NPs, SiO<sub>2</sub>-V NPs.<sup>52,53</sup> In the second step, the previously immobilized vinyl groups worked as coupling agents to introduce reactive groups onto the particle surface and the PNIPAm was then grafted-on using these groups. This synthesis methodology allowed us to obtain core-brush SiO<sub>2</sub> NPs covered with PNIPAm brushes of controlled thickness.

In this type of experimental process, the postulated mechanism of polymer chain grafting on the silica surface consists of two main steps. First, a polymeric radical formed in solution reacts with the immobilized double bond, generating a new reactive surface site from which the new chain growth can be subsequently initiated (see Scheme S1).<sup>54–56</sup> In our previous report, we demonstrated that the selection of the synthetic route is key to the control of crucial characteristics of silica-brush NPs such as grafted polymer density, dispersion, and colloidal stability.<sup>15</sup> In addition, noncontrolled radical polymerizations generally present some advantages at the moment of polymer grafting into surfaces; for example, they involve simple equipment, low cost of processing, and fast

reaction rate and therefore, they are the most viable from an industrial scalability point of view.<sup>57,58</sup>

Table 1 summarizes the synthetic parameters evaluated in order to maximize the grafted polymer content on the SiO<sub>2</sub> NPs surface. The evaluated conditions were final concentration of SiO<sub>2</sub> NPs in the reaction suspension ( $C_{NP}$ ), molar ratio between NIPA and organosilane (N/VTES), type of initiator (i) and molar ratio of initiator with respect to the monomer (i/N). The same SiO<sub>2</sub>-V NPs batch was used in all PNIPAm grafting reactions, so concentration of surface reactive sites was the same for all samples.

Figure 1 presents TEM images of silica nanoparticles before and after PNIPAm photografting in the A<sub>D</sub> conditions, where individual NPs can be observed in addition to those grouped for capillary forces by TEM high vacuum conditions. The dense silica NPs presented an average diameter of 124 ± 11 nm (see Figure 1i). After its polymerization, the core-brush type hybrid structure could be clearly distinguished in the TEM images: a darker gray core of silica was surrounded by a light gray layer, typical of a polymer layer (Figure 1ii).

DLS provides valuable information on the particle size as well as on the level of aggregation and interaction between them in suspension, through the values of hydrodynamic diameter ( $D_h$ ) and the polydispersity index (PDI). The latter is an experimental observable that gives a direct indication of the monodispersity and dispersibility of the nanoparticles submitted to different synthetic steps. A detailed analysis of the DLS data and models used is provided in the SI. All samples presented in Table 1 led to stable dispersions compatible with monodisperse colloids showing PDI < 0.1 (Figures S6, S7). In addition, the decay curves of the autocorrelation functions (Figure S8) enable us to rule out the presence of both large aggregates and other relaxation processes. The polymer thickness,  $t_{pol}$ , was calculated from the difference of core-brush NPs  $D_h$  in comparison to that of the SiO<sub>2</sub>-V NPs precursor. The PDI of SiO<sub>2</sub>-V (0.054) was similar to that of as synthesized SiO<sub>2</sub> NPs (0.062). This is related to a low size distribution of the dispersing entities in the suspension and indicates that after silanization, the SiO<sub>2</sub>-V remained as individual particles.<sup>59</sup>

After PNIPAm photografting when core-brush NPs were obtained, the particles sizes and the PDI values were similar to the ones of SiO<sub>2</sub> NPs, suggesting that the colloidal stability was conserved and the formation of polydispersed aggregates did not take place (see Table 1, PDI values). Moreover, we are able to relate directly the particle size increase due to the polymeric layer grafting. A comparison of the  $t_{pol}$  for different samples in Table 1 showed that the PNIPAm layer thickness increased with higher NIPA concentration (see  $t_{pol}$  for samples A<sub>B</sub> vs A<sub>B</sub>) and the rise of N/VTES ratio (see  $t_{pol}$  for samples C<sub>B</sub>, B<sub>B</sub>, and A<sub>B</sub>). Considering the mechanism in Scheme S1 and the direct proportionality relationship between polymerization rate and monomer concentration, it was reasonable for us to assume that this occurred because of a higher average molecular weight of the polymeric radical that binds to the double bond (Scheme S1ii) as well as by a faster propagation rate (Scheme S1iii).<sup>60</sup> In addition, a higher  $t_{pol}$  was observed when a lower proportion of photoinitiator (see  $t_{pol}$  sample A<sub>B</sub> vs A<sub>B10</sub>) was used. Moreover, the performance was improved when DMPA was selected instead of BP (see  $t_{pol}$  sample A<sub>B</sub> vs A<sub>D</sub>). It was suggested that an excess of initiator tends to favor chain termination reactions, especially in the case of the relatively stable ketyl radical (HO-C(Ph<sub>2</sub>)·) formed by an H

abstraction by BP (type II photoinitiation).<sup>61</sup> We hypothesize that this fact, added to the great efficiency in radical formation by photo-unimolecular cleavage (type I) mechanism of DMPA, could explain its better performance in polymer brush generation. Finally, when the best parameters were combined (sample A<sub>D</sub>) the polymer layer thickness was maximized. The  $t_{pol}$  value for this sample was 31 ± 5 nm, similar to the  $t_{pol}$  of 27.4 nm reported by Ketelson et al. in the case of methyl methacrylate (MMA) radical polymerization on vinyltrimethoxysilane functionalized colloidal silica, performed through thermal initiation.<sup>56</sup>

FTIR and TGA data were used as qualitative and quantitative techniques for the detection of the presence of polybrushes. Figure 1iii shows the DRIFTS spectra corresponding to SiO<sub>2</sub>, SiO<sub>2</sub>-V, and (SiO<sub>2</sub>-V)-g-PNIPAm sample A<sub>D</sub>, confirming the successful silanization process and the hybrid core-brush preparation. As can be seen in the DRIFTS spectra for all the samples, main bands corresponded to the inorganic core: the wide band around 3800–3200 cm<sup>-1</sup> originated by adsorbed water and hydroxylated Si–OH groups stretching vibrations, the 1640 cm<sup>-1</sup> band attributed to OH groups flexing from the adsorbed water, and the strong bands in the 1200–800 cm<sup>-1</sup> region attributed to the Si–O–Si vibrations. After silanization with VTES, the characteristic bands of the anchored vinyl group were masked by silica core strong vibrations and stretching and deformation vibrations of the C–H bond (1550–1350 cm<sup>-1</sup>), which were originated by alkyl residues of nonhydrolyzed Si–OC<sub>2</sub>H<sub>5</sub> groups during SiO<sub>2</sub> NPs synthesis.<sup>62</sup> After photografting, new bands appeared in the DRIFTS spectrum, which confirms that PNIPAm was successfully grafted on the SiO<sub>2</sub>-V surface. The signals due to the PNIPAm aliphatic chain, –CH<sub>2</sub>– symmetric and antisymmetric stretching modes, were distinguishable at 2929 and 2858 cm<sup>-1</sup>. Moreover, the intensity of the 1500–1430 cm<sup>-1</sup> band assigned to C–H vibrations increases in comparison with that of the SiO<sub>2</sub>-V samples. In addition, an amide group C=O stretching at 1650 cm<sup>-1</sup> was overlapped with the H<sub>2</sub>O adsorbed band. Finally, the N–H bending vibration of the polymer's amide group at 1540 cm<sup>-1</sup> was clearly distinguished. A zoomed in image of the PNIPAm signal region is presented in Figure 1iv for different synthesis conditions of the core-brush NPs. Besides, it was observed that its intensity changed markedly according to core-brush synthesis conditions for the four selected samples; the sample A<sub>D</sub> presented higher intensity, in agreement with the DLS results that lead to thicker brush shells.

In addition, the thermal properties of unmodified and silanized SiO<sub>2</sub> NPs and PNIPAm core-brush NPs were evaluated using TGA (see Figure S1). The weight loss observed for the unmodified SiO<sub>2</sub> heated from room temperature to 800 °C was around 10–15%, mainly due to the removal of water adsorbed to approximately 200 °C and then by the dehydroxylation processes of the Si–OH groups present in the structure of the silica core at  $T > 400$  °C.<sup>50</sup> After the silanization of SiO<sub>2</sub> with VTES, the mass loss was higher, as expected, due to the functional groups that were immobilized on the surface, while the profile of mass loss did not show significant differences in comparison with bare silica NPs. In case of PNIPAm core-brush NPs, a second mass loss was observed starting around 200 °C, due to the progressive thermal decomposition of the organic content. This takes place in several closely related and nondistinguishable stages, making it difficult to specifically assign them to the loss of polymer

fragments such as monomers, dimers, etc. From 600 °C until the end of the assay, masses remained constant. The organic content of each system as well as the organic content reached in each synthetic step were calculated taking into account the weight loss that occurred from 200 °C.

From TGA results and eqs S1 and S2 (See SI), the grafting percentage (%G) and the estimated number of functional groups anchored on the surface per unit area ( $N_{\text{exp}}$ ) were estimated for selected core-brush NPs. For SiO<sub>2</sub>-V NPs,  $N_{\text{exp}}$  was 17.2; this high density of vinyl groups per unit area indicates that after the surface functionalization, multiple layers of vinylsilane were obtained, probably like polycondensate networks: a typical result in aqueous reaction media.<sup>63</sup> In Table 2, the values corresponding to the PNIPAm content

**Table 2. Estimated Number of Surface Grafted Groups Per Area Unit,  $N_{\text{exp}}$ , and Grafting Percentage, %G, Calculated from TGA Experiments**

Sample	%G	$N_{\text{exp}}$ (nm <sup>-2</sup> )
C <sub>B</sub>	2.3	5.3
B <sub>B</sub>	2.6	6.0
A <sub>B</sub>	3.2	7.6
A <sub>D</sub>	3.4	8.2

reached for selected samples are presented. It can be seen that when photopolymerization conditions were optimized, an increase in %G was achieved, which correlated very well with DLS and FTIR results. For the sample with the highest polymer content, sample A<sub>D</sub>, the %G value was 3.4, which corresponds to a  $N_{\text{exp}}$  of 8.2 NIPA molecules per nm<sup>2</sup>. This surface density of the grafted monomer units is in the same order of magnitude as that reported by Ketelson et al.<sup>56</sup> In summary, the best grafting conditions were obtained in the case of sample G, C<sub>NP</sub>: 0.5%, molar ratio N/VTES: 40, type of initiator: DMPA, % molar ratio i/N: 1.

**Core-Shell-Brush Nanosystems Preparation.** Scheme 2 shows the synthetic methodology carried out for obtaining hybrid colloids with a plasmonic core. The synthesis of spherical gold NPs with diameter closer to 15 nm (Au NPs) was performed following the well-known Turkevich method based on the Au precursor reduction using sodium citrate.<sup>64</sup> For core-shell NPs preparation with dense silica layer, Au@SiO<sub>2</sub>, the Au colloid was transferred into a typical Stöber medium, after citrate exchanging by the polymeric amphiphilic stabilizer PVP.<sup>65</sup> A postsynthesis solvothermal treatment was carried out at 60 °C in order to achieve a higher consolidation degree of the silica structure and improve its stability against dissolution.

Subsequently, surface hybrid Au@SiO<sub>2</sub> NPs were functionalized with vinyl groups by a VTES silanization process similar to the one previously described. Finally, PNIPAm brushes were

grafted on its surface according to the previously optimized methodology, using sample A<sub>D</sub> conditions. This multistage synthesis allowed us to obtain complex hybrid nanostructures as a stable colloidal system.

Figure 2 shows TEM micrographs of hybrid NPs before and after the grafting of PNIPAm brushes. For core-shell NPs containing a plasmonic core and dense silica shell (sample Au@SiO<sub>2</sub>, Figure 2i), monodispersity was observed, with an average total diameter of 74 ± 4 nm having a single metallic core in approximately 70% of the NPs. After PNIPAm photopolymerization, monodisperse particles with a double shell were clearly observed (Figure 2ii).

In addition, Figure 2iii presents the UV–vis spectra for the hybrid NPs at the different synthesis steps mentioned before. The maximum attributed to the Localized Surface Plasmon Resonance (LSPR) for citrate stabilized Au NPs was around 519 nm, as previously reported.<sup>64</sup> In Figure 2iii, a change in  $\lambda_{\text{max}}$  was observed from 519 to 522 and 528 nm when the Au NP was surrounded by citrate molecules, then by the PVP polymer, and by the compact silica shell, respectively. As previously mentioned, the LSPR band location varies when modifying the immediate environment of plasmonic NP; specifically, the absorbance maximum,  $\lambda_{\text{max}}$ , experiences a slight bathochromic shift when the surrounding medium refractive index is increased.<sup>30</sup> After the graft polymerization was performed,  $\lambda_{\text{max}}$  did not change. This result was attributed to the fact that a second hybrid layer on Au NP has much less influence on the plasmon resonance position, due to the longer distance to the plasmonic surface. It is important to notice that in all spectra, the plasmonic band conserves the shape and wavelength range of the original Au NPs, indicating that the successive surface modifications did not produce an extended aggregation of the colloid.

In addition, a luminescent silica shell can be prepared by the addition of tris(bipyridine)ruthenium(II), Ru(bpy)<sub>3</sub><sup>2+</sup>, in the Stober reaction mixture. Figure S3 shows the steady-state emission spectrum of Au@SiO<sub>2</sub>/Ru(bpy)<sub>3</sub><sup>2+</sup> NPs and indicates that the complex has indeed been entrapped in the SiO<sub>2</sub> matrix during the formation of the shell. This behavior makes the nanosystems ideal for bioimaging or theranostics, opening a new gate for functional integration.

**Thermoresponsiveness Behavior.** The thermosensitivity of the as-prepared complex hybrid nanosystems was investigated by performing DLS experiments.

At first, polymer thickness,  $t_{\text{pol}}$ , was evaluated by DLS at extremes temperatures from PNIPAm LCST. Figure 3 shows the  $t_{\text{pol}}$  results of aqueous colloidal suspensions for sample A<sub>D</sub> and Au@SiO<sub>2</sub>-g-PNIPAm at 10 and 40 °C. In both cases, when the temperature solution was lower than LCST (10 °C) the obtained  $t_{\text{pol}}$  was higher than when temperature was above the LCST (40 °C). This can be interpreted as a consequence of PNIPAm brushes collapsing due to the phase transition from a

**Scheme 2. Synthesis Methodology of Core-Shell Au@SiO<sub>2</sub> and Nanoparticles and Core-Shell-Brush Nanosystems, Au@SiO<sub>2</sub>-g-PNIPAm**



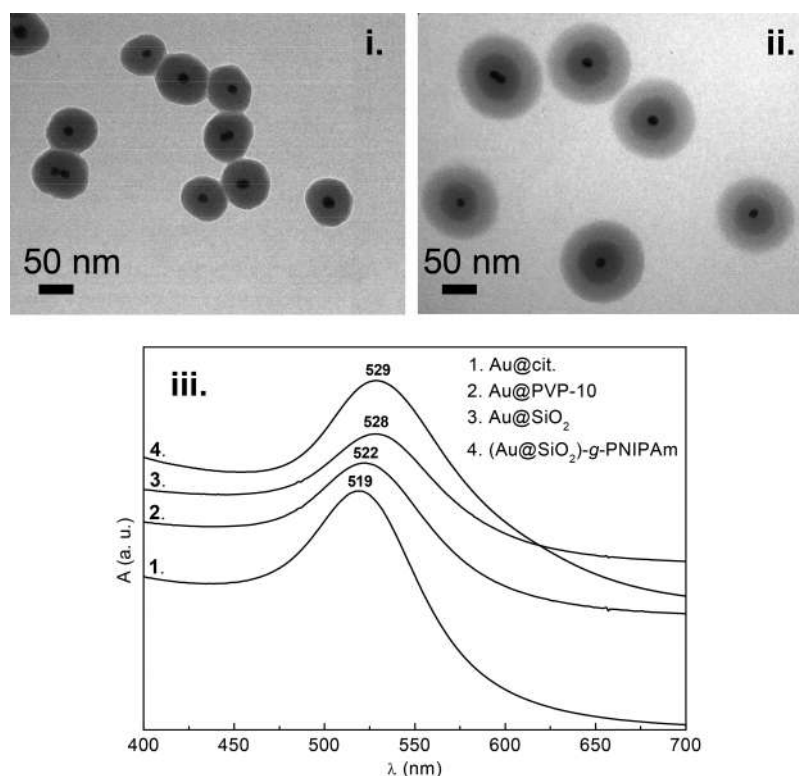


**Figure 2.** TEM images of NPs (i) Au@SiO<sub>2</sub>, (ii) Au@SiO<sub>2</sub>-g-PNIPAm, and (iii) UV-vis spectra of Au NPs, Au@SiO<sub>2</sub> at different reactions steps, as indicated in the labels.

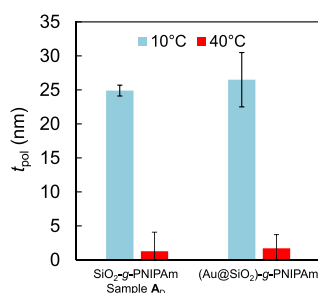


**Figure 3.** Polymer thickness ( $t_{pol}$ ) studied by DLS below and above PNIPAm LCST for Sample A<sub>D</sub> and Au@SiO<sub>2</sub>-g-PNIPAm.

hydrophobic to a hydrophilic state in aqueous solution. A detailed analysis of the DLS experiments is provided in the SI, Figures S6 and S7.

As was mentioned in the introduction, the exposure of Au nanocarriers to an external light source leads to strong absorption at a specific wavelength, which is referred to as LSPR.<sup>10,66–68</sup> In order to induce the PNIPAm thermoresponsiveness by efficient light absorption and fast heat conversion caused for Au LSPR excitation, a DLS experiment using sample Au@SiO<sub>2</sub>-g-PNIPAm was performed coupling a commercial green LED lamp (5W  $\lambda = 530$  nm), as seen in Figure 4i.

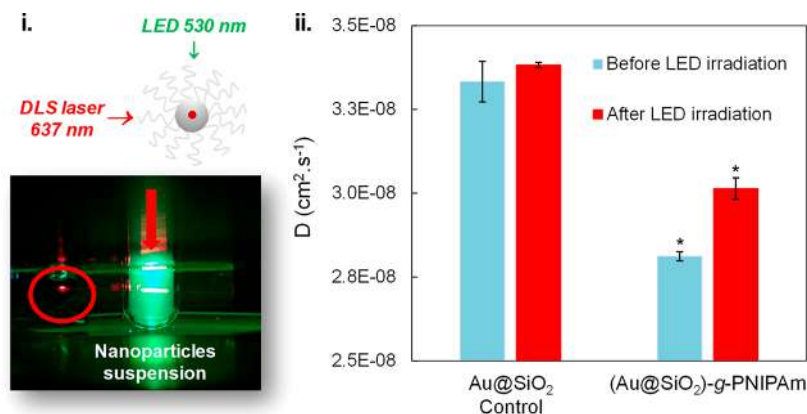


**Figure 4.** (i) DLS experiment setup using sample Au@SiO<sub>2</sub>-g-PNIPAm. (ii) Diffusion coefficient obtained by DLS experiments before and after irradiation of Au@SiO<sub>2</sub> (control) and Au@SiO<sub>2</sub>-g-PNIPAm colloid suspension with a commercial green LED lamp. The corresponding autocorrelation functions (ACF) are presented in SI, Figure S8. Statistical differences between groups were calculated by applying ANOVA and Tukey post test,  $P < 0.05$ .

The heat produced by LSPR irradiation was evaluated on a bare Au NPs colloidal suspension. An increase of around 6 °C from room temperature after 15 min of irradiation with a green LED was observed; this period was enough to appreciate a difference in the temperature effect between the dispersions containing Au NP species and those without Au NP species (see SI Table S1). The same temperature increase was detected when a Au@SiO<sub>2</sub> NPs colloidal suspension was irradiated under the same conditions, suggesting that the silica shell did not affect the heat conversion. It is important to notice that when water was irradiated, a smaller temperature increment was sensed (2 °C); this means that the temperature rise on Au and Au@SiO<sub>2</sub> was a consequence of light absorption and fast heat conversion caused by Au LSPR excitation with the green commercial LED lamp employed.

Afterward, LED lamp irradiation was combined with the DLS experiment. DLS is a technique that measures directly the diffusion coefficient ( $D_h$ ) of the colloidal particles from time intensity autocorrelation functions due to fluctuations of the scattered light in an observation volume. At constant temperature, as the solvent's viscosity is fixed, the hydrodynamic radius of the dispersed colloids is easily obtained through the Stokes–Einstein relationship assuming a spherical shape

$$D = \frac{kT}{6\pi\eta r} \quad (1)$$

where  $D$  is the diffusion coefficient,  $k$  is Boltzmann constant,  $T$  is temperature,  $\eta$  is viscosity, and  $r$  is the hydrodynamic ratio in eq 1. Hence, when Au@SiO<sub>2</sub> based NP are irradiated with green light, we should expect a temperature change of the surrounding solvent. In fact, Schaertl and Roos reported convection and thermodiffusion of Au NPs during DLS experiments but with the usage of a very high power laser for plasmon absorption and scattering (Ar+ laser, 250–500 mW output power).<sup>69</sup> Nonetheless, in our case, the light scattering autocorrelation function obtained for Au@SiO<sub>2</sub>-g-PNIPAm NPs fits a simple exponential decay, suggesting that thermoconvection can be disregarded.

As temperature measurement in the scattering volume proved to be highly problematic, we decided to refer the hydrodynamic changes after LED irradiation to the diffusion coefficients ( $D$ ) of the particles, which is an unbiased measurement of a DLS experiment. Moreover, a simple calculation in eq 1, using the temperature dependence of the water viscosity and assuming a constant hydrodynamic radius for an ideal nanoparticle, reveals that the difference expected in the diffusion coefficients values for a  $\Delta T = 2$  °C lies around 1% ( $\eta_{\text{H}_2\text{O}, 20\text{ }^\circ\text{C}} = 1$  mPa s and  $\eta_{\text{H}_2\text{O}, 22\text{ }^\circ\text{C}} = 0.9544$  mPa s). When this temperature difference is increased to  $\Delta T = 5$  °C, the change in the diffusion coefficients relation is now 1.1% ( $\eta_{\text{H}_2\text{O}, 22\text{ }^\circ\text{C}} = 0.9544$  mPa s and  $\eta_{\text{H}_2\text{O}, 25\text{ }^\circ\text{C}} = 0.8900$  mPa s). Clearly, temperature and solvent viscosity changes in this range do not alter significantly the relation between the diffusion coefficients as long as the particle size does not change. Thus,  $D$  was obtained before and after 15 min of LED irradiation on Au@SiO<sub>2</sub>-g-PNIPAm colloidal suspension. An Au@SiO<sub>2</sub> sample was employed as control, which showed the same temperature increase and in which it can be safely assumed that no change in particle size takes place.

The results obtained are presented in Figure 4ii. For the control sample, even though the temperature increased around 6 °C, the diffusion coefficient did not present significant

differences after LED irradiation using Tukey's Multiple Comparison Test,  $P < 0.05$ . While, in the case of sample Au@SiO<sub>2</sub>-g-PNIPAm, diffusion coefficient increased after LED irradiation. Taking into account the heat produced by LED irradiation and the diffusion coefficient rise that was observed, we assumed that PNIPAm thermoresponsiveness was activated producing a smaller hydrodynamic ratio, and consequently, the particles presented higher mobility and diffusion.

After irradiation with the LED lamp, we observed a small variation in the hydrodynamic diameter of the Au@SiO<sub>2</sub> NPs ( $\Delta \sim 1.2$  nm,  $118.5 \pm 2.1$  vs  $117.3 \pm 0.7$ ). However, this difference is not statistically relevant as Tukey test points. In contrast, when the same treatment was applied to Au@SiO<sub>2</sub>-g-PNIPAm NPs, a decrease in size of 9.3 nm ( $140.4 \pm 0.7$  vs  $131.1 \pm 1.5$ ) can be considered a statistically significant difference. In this case, we attribute this behavior to the contraction of the PNIPAm thermoresponsive external polymer layer. This variation corresponds to a  $\sim 6\%$  change of the total diameter of the NPs but  $\sim 37\%$  of the total contraction of the polymeric layer (see Figure 3, right). The latter is consistent with the magnitude of the variation of the thickness of the polymer layer in the temperature range increased by a photothermal effect during the irradiation treatment (initial  $T$ : 18.5 °C and final  $T$ : 20.9 °C); see thickness vs temperature plots in Figure S3.

## CONCLUSIONS

We report a reproducible and simple sequential one-pot method for obtaining core-shell-brush nanosystems with light-induced size change through thermoplasmonics transduction. This strategy is based on a controlled sequence of orthogonal processes in one-pot conditions: precipitation, coating, and radical photopolymerization; these allow us to synthesize hybrid nanosystems based on a monodisperse silica nanoparticle platform to which surface PNIPAm brushes are added. In order to maximize the polymeric layer thickness, the polymerization parameters were optimized on dense silica NPs, leading to a 15 nm thickness polymer layer that presented significant shrinkage upon heating above the LCST. The methodology was successfully transferred to PNIPAm brush grafting on plasmonic core-shell NPs with a gold core and dense silica layers, which preserved the system colloidal stability. For this three-layer nanosystem, we demonstrated that the thermoresponsiveness was efficiently induced by LSPR excitation through *in situ* DLS measurements.

It is also important to stress that we reported for the first time a new methodology for studying *in situ* the thermo-response activation by plasmonic irradiation. These light-remote controlled thermoresponsive hybrid nanosystems are composed of three modular components: Au (plasmon heating module), silica (stabilizes the metal and compatibilizes the surface chemistry), and PNIPAm brushes (thermo-responsive domain). In order to validate our findings, the light-to-heat induced shrinkage was evaluated using DLS under LED irradiation.

As an outlook for future developments, the modular features of this kind of multilayered particles can be further exploited for the design of tunable nanosystems. All three modules can be modified at will to tune either the plasmonic excitation wavelength or the LCST. The silica middle layer can also be modified to include other functional groups, mesopores, or fluorescent tracking species, as was demonstrated with Ru(bpy)<sub>3</sub><sup>2+</sup>, opening the gate for bioimaging or theranostics.

Although PNIPAm microgels have been exhaustively studied, it is important to notice that in this work, the PNIPAm is integrated into a light-controllable nanosystem with excellent colloidal stability and dispersibility. We anticipate that the versatility of this platform with photothermo-physical transduction has broad potential applications in smart drug or gene carriers, theranostics, and responsive bioscaffolds for tissue engineering or soft robotics.

## ■ ASSOCIATED CONTENT

### SI Supporting Information

The Supporting Information is available free of charge at <https://pubs.acs.org/doi/10.1021/acs.langmuir.9b03065>.

Detailed experimental methods, polymer characterization, thermo-responsiveness, selection of LED time irradiation, responsiveness reversibility, luminescent tris(bipyridine)ruthenium(II)-doped silica shell, DLS data information (PDF)

## ■ AUTHOR INFORMATION

### Corresponding Authors

**Cintia Belén Contreras** – Instituto de Nanosistemas, Universidad Nacional de San Martín-CONICET, Buenos Aires 1650, Argentina; Instituto de Investigaciones Físicoquímicas Teóricas y Aplicadas, Universidad Nacional de La Plata-CONICET, La Plata, Buenos Aires B1900, Argentina; [orcid.org/0000-0003-3956-0788](https://orcid.org/0000-0003-3956-0788); Email: [ccontreras@unsam.edu.ar](mailto:ccontreras@unsam.edu.ar)

**Galo J.A.A. Soler-Illia** – Instituto de Nanosistemas, Universidad Nacional de San Martín-CONICET, Buenos Aires 1650, Argentina; [orcid.org/0000-0001-9984-3806](https://orcid.org/0000-0001-9984-3806); Email: [gsoler-illia@unsam.edu.ar](mailto:gsoler-illia@unsam.edu.ar)

### Authors

**María Jazmín Penelas** – Instituto de Nanosistemas, Universidad Nacional de San Martín-CONICET, Buenos Aires 1650, Argentina; Gerencia Química & Instituto de Nanociencia y Nanotecnología, Centro Atómico Constituyentes, Comisión Nacional de Energía, CONICET, 1650, Buenos Aires, Argentina

**Paula C. Angelomé** – Gerencia Química & Instituto de Nanociencia y Nanotecnología, Centro Atómico Constituyentes, Comisión Nacional de Energía, CONICET, 1650, Buenos Aires, Argentina; [orcid.org/0000-0002-4402-5045](https://orcid.org/0000-0002-4402-5045)

**Alejandro Wolosiuk** – Gerencia Química & Instituto de Nanociencia y Nanotecnología, Centro Atómico Constituyentes, Comisión Nacional de Energía, CONICET, 1650, Buenos Aires, Argentina; [orcid.org/0000-0003-0854-9949](https://orcid.org/0000-0003-0854-9949)

**Omar Azzaroni** – Instituto de Investigaciones Físicoquímicas Teóricas y Aplicadas, Universidad Nacional de La Plata-CONICET, La Plata, Buenos Aires B1900, Argentina; [orcid.org/0000-0002-5098-0612](https://orcid.org/0000-0002-5098-0612)

Complete contact information is available at: <https://pubs.acs.org/doi/10.1021/acs.langmuir.9b03065>

### Author Contributions

<sup>§</sup>Both authors contributed equally to this work

### Notes

The authors declare no competing financial interest.

## ■ ACKNOWLEDGMENTS

This work was made possible thanks to funding from UNSAM, ANPCyT (PICT-2014-3687 934, PICT 2015-0351, 2015-3526 and 2017-4651), and a CONICET-DFG joint project (MU 1674#15-1). Authors are also grateful to Lucila Morono for her TEM assistance. M.J.P and C.B.C acknowledge doctoral and postdoctoral fellowships from CONICET and UNSAM.

## ■ REFERENCES

- (1) Chen, G.; Roy, I.; Yang, C.; Prasad, P. N. *Nanochemistry and Nanomedicine for Nanoparticle-Based Diagnostics and Therapy*. *Chem. Rev.* **2016**, *116* (5), 2826–2885.
- (2) Sozer, N.; Kokini, J. L. Nanotechnology and Its Applications in the Food Sector. *Trends Biotechnol.* **2009**, *27*, 82–89.
- (3) López-Lorente, A. I.; Valcárcel, M. Analytical Nanoscience and Nanotechnology. In *Gold Nanoparticles in Analytical Chemistry*; Elsevier: 2014; pp 1–35.
- (4) Loos, M. Nanoscience and Nanotechnology. In *Carbon Nanotube Reinforced Composites*; Elsevier: 2015; pp 1–36.
- (5) Brown, P.; Eral, H. B. *Chapter 12 - Smart and Stimuli-Responsive Colloids*; **2016**.389
- (6) Lee, W.; Kim, D.; Lee, S.; Park, J.; Oh, S.; Kim, G.; Lim, J.; Kim, J. Stimuli-Responsive Switchable Organic-Inorganic Nanocomposite Materials. *Nano Today* **2018**, *23*, 97–123.
- (7) Raza, A.; Hayat, U.; Rasheed, T.; Bilal, M.; Iqbal, H. M. N. Light-Responsive Drug Delivery Systems for Cancer Treatment: A Review. *Eur. J. Med. Chem.* **2018**, *3*, 1–13.
- (8) Mishra, P.; Nayak, B.; Dey, R. K. PEGylation in Anti-Cancer Therapy: An Overview. *Asian J. Pharm. Sci.* **2016**, *11* (3), 337–348.
- (9) Slowing, I. I.; Trewyn, B. G.; Giri, S.; Lin, V. S. Y. Mesoporous Silica Nanoparticles for Drug Delivery and Biosensing Applications. *Adv. Funct. Mater.* **2007**, *17* (8), 1225–1236.
- (10) Shagan, A.; Croitoru-Sadger, T.; Corem-Salkmon, E.; Mizrahi, B. Near-Infrared Light Induced Phase Transition of Biodegradable Composites for On-Demand Healing and Drug Release. *ACS Appl. Mater. Interfaces* **2018**, *10* (4), 4131–4139.
- (11) Strover, L. T.; Malmström, J.; Laita, O.; Reynisson, J.; Aydemir, N.; Nieuwoudt, M. K.; Williams, D. E.; Dunbar, P. R.; Brimble, M. a.; Travas-Sejdic, J. A New Precursor for Conducting Polymer-Based Brush Interfaces with Electroactivity in Aqueous Solution. *Polymer* **2013**, *54*, 1305–1317.
- (12) Ballauff, M.; Lu, Y. Smart<sup>®</sup> Nanoparticles: Preparation, Characterization and Applications. *Polymer* **2007**, *48*, 1815–1823.
- (13) Fu, X.; Hosta-Rigau, L.; Chandrawati, R.; Cui, J. Multi-Stimuli-Responsive Polymer Particles, Films, and Hydrogels for Drug Delivery. *Chem* **2018**, *4*, 1–24.
- (14) Sun, Y.; Sai, H.; Spoth, K. A.; Tan, K. W.; Werner-Zwanziger, U.; Zwanziger, J.; Gruner, S. M.; Kourkoutis, L. F.; Wiesner, U. Stimuli-Responsive Shapeshifting Mesoporous Silica Nanoparticles. *Nano Lett.* **2016**, *16*, 651–655.
- (15) Penelas, M. J.; Contreras, C. B.; Giussi, J.; Wolosiuk, A.; Azzaroni, O.; Soler Illia, G. J. A. A. Controlling Dispersion, Stability and Polymer Content on PDEGMA-Functionalized Core-Brush Silica Colloids. *Colloids Surf, A* **2019**, *574*, 12–20.
- (16) Thanh, T.; Thi, H.; Cao, V. Du; Nhu, T.; Nguyen, Q.; Hoang, D. T.; Ngo, V. C.; Nguyen, D. H. Functionalized Mesoporous Silica Nanoparticles and Biomedical Applications. *Mater. Sci. Eng., C* **2019**, *99*, 631–656.
- (17) Ha, C.-S. Polymer Based Hybrid Nanocomposites; A Progress Toward Enhancing Interfacial Interaction and Tailoring Advanced Applications. *Chem. Rec.* **2018**, *18* (7–8), 759–775.
- (18) Soler-Illia, G. J. A. A.; Azzaroni, O. Multifunctional Hybrids by Combining Ordered Mesoporous Materials and Macromolecular Building Blocks. *Chem. Soc. Rev.* **2011**, *40*, 1107.
- (19) Contreras, C. B.; Azzaroni, O.; Soler-Illia, G. J. A. A. Use of Confinement Effects in Mesoporous Materials to Build Tailored Nanoarchitectures. *Compr. Nanosci. Nanotechnol.* **2019**, 331–348.

- (20) Alberti, S.; Soler-Illia, G. J. A. A.; Azzaroni, O. Gated Supramolecular Chemistry in Hybrid Mesoporous Silica Nanoarchitectures: Controlled Delivery and Molecular Transport in Response to Chemical, Physical and Biological Stimuli. *Chem. Commun.* **2015**, *51*, 6050–6075.
- (21) Timko, B. P.; Dvir, T.; Kohane, D. S. Remotely Triggerable Drug Delivery Systems. *Adv. Mater.* **2010**, *22*, 4925–4943.
- (22) Said, S. S.; Campbell, S.; Hoare, T. Externally-Addressable Smart Drug Delivery Vehicles: Current Technologies and Future Directions. *Chem. Mater.* **2019**, *31*, 4971–4989.
- (23) Xia, Y.; Xiong, Y.; Lim, B.; Skrabalak, S. E. Shape-Controlled Synthesis of Metal Nanocrystals: Simple Chemistry Meets Complex Physics? *Angew. Chem., Int. Ed.* **2009**, *48*, 60–103.
- (24) Xia, Y.; Gilroy, K. D.; Peng, H.-C.; Xia, X. Seed-Mediated Growth of Colloidal Metal Nanocrystals. *Angew. Chem., Int. Ed.* **2017**, *56*, 60–95.
- (25) Bashir, S.; Liu, J. Nanomaterials and Their Application. In *Advanced Nanomaterials and their Applications in Renewable Energy* **2015**, 1–50.
- (26) Zhou, J.; Ralston, J.; Sedev, R.; Beattie, D. A. Functionalized Gold Nanoparticles: Synthesis, Structure and Colloid Stability. *J. Colloid Interface Sci.* **2009**, *331*, 251–262.
- (27) Zhao, P.; Li, N.; Astruc, D. State of the Art in Gold Nanoparticle Synthesis. *Coord. Chem. Rev.* **2013**, *257*, 638–665.
- (28) Saneja, A.; Kumar, R.; Arora, D.; Kumar, S.; Panda, A. K.; Jaglan, S. Recent Advances in Near-Infrared Light-Responsive Nanocarriers for Cancer Therapy. *Drug Discovery Today* **2018**, *23*, 1115–1125.
- (29) Saroj, S.; Rajput, S. J. Journal of Drug Delivery Science and Technology Composite Smart Mesoporous Silica Nanoparticles as Promising Therapeutic and Diagnostic Candidates: Recent Trends and Applications. *J. Drug Delivery Sci. Technol.* **2018**, *44*, 349–365.
- (30) Hanske, C.; Sanz-Ortiz, M. N.; Liz-Marzán, L. M. Silica-Coated Plasmonic Metal Nanoparticles in Action. *Adv. Mater.* **2018**, *30*, 1–28.
- (31) Rzaev, Z. M. O.; Dinçer, S.; Pişkin, E. Functional Copolymers of N-Isopropylacrylamide for Bioengineering Applications. *Prog. Polym. Sci.* **2007**, *32*, 534–595.
- (32) Cuggino, J. C.; Contreras, C. B.; Jimenez-Kairuz, A.; Maletto, B. A.; Alvarez Igarzabal, C. I. Novel Poly(NIPA-Co-AAc) Functional Hydrogels with Potential Application in Drug Controlled Release. *Mol. Pharmaceutics* **2014**, *11*, 2239–2249.
- (33) Lu, Y.; Ballauff, M. Thermosensitive Core-Shell Microgels: From Colloidal Model Systems to Nanoreactors. *Prog. Polym. Sci.* **2011**, *36*, 767–792.
- (34) Ballauff, M.; Lu, Y. Smart<sup>2</sup> Nanoparticles: Preparation, Characterization and Applications. *Polymer* **2007**, *48*, 1815–1823.
- (35) Wu, S.; Dzubiella, J.; Kaiser, J.; Drechsler, M.; Guo, X.; Ballauff, M.; Lu, Y. Thermosensitive Au-PNIPA Yolk-Shell Nanoparticles with Tunable Selectivity for Catalysis. *Angew. Chem., Int. Ed.* **2012**, *51*, 2229–2233.
- (36) Shen, S.; Ding, B.; Zhang, S.; Qi, X.; Wang, K.; Tian, J.; Yan, Y.; Ge, Y.; Wu, L. Near-Infrared Light-Responsive Nanoparticles with Thermosensitive Yolk-Shell Structure for Multimodal Imaging and Chemo-Photothermal Therapy of Tumor. *Nanomedicine* **2017**, *13*, 1607–1616.
- (37) Ma, K.; Wiesner, U. Ultra-Small Sub-10 Nm Near Infrared Fluorescent Mesoporous Silica Nanoparticles. *J. Am. Chem. Soc.* **2012**, *134*, 1–10.
- (38) Ma, K.; Mendoza, C.; Hanson, M.; Werner-Zwanziger, U.; Zwanziger, J.; Wiesner, U. Control of Ultrasmall Sub-10 Nm Ligand-Functionalized Fluorescent Core-Shell Silica Nanoparticle Growth in Water. *Chem. Mater.* **2015**, *27*, 4119–4133.
- (39) Sun, Y.; Sai, H.; von Stein, F.; Riccio, M.; Wiesner, U. Water-Based Synthesis of Ultrasmall PEGylated Gold-Silica Core-Shell Nanoparticles with Long-Term Stability. *Chem. Mater.* **2014**, *26*, 5201–5207.
- (40) Xu, J.; Perry, C. C. A Novel Approach to Au@SiO<sub>2</sub> Core-Shell Spheres. *J. Non-Cryst. Solids* **2007**, *353*, 1212–1215.
- (41) Nakamura, T.; Yamada, Y.; Yano, K. Direct Synthesis of Monodispersed Thiol-Functionalized Nanoporous Silica Spheres and Their Application to a Colloidal Crystal Embedded with Gold Nanoparticles. *J. Mater. Chem.* **2007**, *17*, 3726.
- (42) Chen, J.; Zhang, R.; Han, L.; Tu, B.; Zhao, D. One-Pot Synthesis of Thermally Stable Gold@ Mesoporous Silica Core-Shell Nanospheres with Catalytic Activity. *Nano Res.* **2013**, *6*, 871–879.
- (43) Tian, J.; Huang, B.; Zhang, W. Precise Self-Assembly and Controlled Catalysis of Thermoresponsive Core-Satellite Multi-component Hybrid Nanoparticles. *Langmuir* **2019**, *35*, 266–275.
- (44) Wang, Y.; Wang, L.; Hao, J.; Dong, S. Plasmonic Core-Shell Ionic Microgels for Photo-Tuning Catalytic Applications. *New J. Chem.* **2018**, *42*, 2149–2157.
- (45) Villaverde, G.; Gómez-Graña, S.; Guisasaola, E.; García, I.; Hanske, C.; Liz-Marzán, L. M.; Baeza, A.; Vallet-Regí, M. Targeted Chemo-Photothermal Therapy: A Nanomedicine Approximation to Selective Melanoma Treatment. *Part. Part. Syst. Charact.* **2018**, *35*, 1–10.
- (46) Azzaroni, O.; Szeleifer, I. *Polymer and Biopolymer Brushes: For Materials Science and Biotechnology, First ed.*; JohnWiley & Sons: Hoboken, 2018.
- (47) Yameen, B.; Ali, M.; Álvarez, M.; Neumann, R.; Ensinger, W.; Knoll, W.; Azzaroni, O. A Facile Route for the Preparation of Azide-Terminated Polymers. “Clicking” Polyelectrolyte Brushes on Planar Surfaces and Nanochannels. *Polym. Chem.* **2010**, *1*, 183–192.
- (48) Cui, J.; Nguyen, T.-H.; Ceolin, M.; Berger, R.; Azzaroni, O.; del Campo, A. Phototunable Response in Caged Polymer Brushes. *Macromolecules* **2012**, *45*, 3213–3220.
- (49) Calvo, A.; Yameen, B.; Williams, F. J.; Azzaroni, O.; Soler-Illia, G. J. A. A. Facile Molecular Design of Hybrid Functional Assemblies with Controllable Transport Properties: Mesoporous Films Meet Polyelectrolyte Brushes. *Chem. Commun.* **2009**, *18*, 2553–2555.
- (50) Bogush, G. H.; Tracy, M. A.; Zukoski, C. F. Preparation of Monodisperse Silica Particles: Control of Size and Mass Fraction. *J. Non-Cryst. Solids* **1988**, *104*, 95–106.
- (51) Stöber, W.; Fink, A.; Bohn, E. Controlled Growth of Monodisperse Silica Spheres in the Micron Size Range. *J. Colloid Interface Sci.* **1968**, *26*, 62–69.
- (52) Shin, Y.; Lee, D.; Lee, K.; Ahn, K. H.; Kim, B. Surface Properties of Silica Nanoparticles Modified with Polymers for Polymer Nanocomposite Applications. *J. Ind. Eng. Chem.* **2008**, *14*, 515–519.
- (53) Penelas, M. J.; Soler-Illia, G. J. A. A.; Levi, V.; Bordoni, A. V.; Wolosiuk, A. Click-Based Thiol-Ene Photografting of COOH Groups to SiO<sub>2</sub> Nanoparticles: Strategies Comparison. *Colloids Surf., A* **2019**, *562*, 61–70.
- (54) Tsubokawa, N.; Kimoto, T.; Koyama, K. Polymerization of Vinyl Monomers in the Presence of Silica Having Surface Functional Groups. *Colloid Polym. Sci.* **1993**, *271*, 940–946.
- (55) Bialk, M.; Prucker, O.; Rühle, J. Grafting of Polymers to Solid Surfaces by Using Immobilized Methacrylates. *Colloids Surf., A* **2002**, *198*, 543–549.
- (56) Ketelson, H. A.; Brook, M. A.; Pelton, R. H. Sterically Stabilized Silica Colloids: Radical Grafting of Poly(Methyl Methacrylate) and Hydrosilylative Grafting of Silicones to Functionalized Silica. *Polym. Adv. Technol.* **1995**, *6*, 335–344.
- (57) Kim, S.; Kim, E.; Kim, S.; Kim, W. Surface Modification of Silica Nanoparticles by UV-Induced Graft Polymerization of Methyl Methacrylate. *J. Colloid Interface Sci.* **2005**, *292*, 93–98.
- (58) Zhou, Q.; Luo, W.; Zhang, X. Ingenious Route for Ultraviolet-Induced Graft Polymerization Achieved on Inorganic Particle: Fabricating Magnetic Poly(Acrylic Acid) Densely Grafted Nanocomposites for Cu<sup>2+</sup> Removal. *Appl. Surf. Sci.* **2017**, *413*, 181–190.
- (59) Schärfl, W. *Light Scattering from Polymer Solutions and Nanoparticle Dispersions*, 1st ed.; Springer-Verlag Berlin Heidelberg: 2007.
- (60) Nguyen, V.; Yoshida, W.; Cohen, Y. Graft Polymerization of Vinyl Acetate onto Silica. *J. Appl. Polym. Sci.* **2003**, *87*, 300–310.

- (61) Yagci, Y.; Jockusch, S.; Turro, N. J. Photoinitiated Polymerization: Advances, Challenges, and Opportunities. *Macromolecules* **2010**, *43*, 6245–6260.
- (62) van Blaaderen, A.; Kentgens, A. P. M. Particle Morphology and Chemical Microstructure of Colloidal Silica Spheres Made from Alkoxysilanes. *J. Non-Cryst. Solids* **1992**, *149*, 161–178.
- (63) Fadeev, A. Y.; McCarthy, T. J. Self-Assembly Is Not the Only Reaction Possible between Alkyltrichlorosilanes and Surfaces: Monomolecular and Oligomeric Covalently Attached Layers of Dichloro- and Trichloroalkylsilanes on Silicon. *Langmuir* **2000**, *16*, 7268–7274.
- (64) Turkevich, J.; Stevenson, P. C.; Hillier, J. A Study of the Nucleation and Growth Processes in the Synthesis of Colloidal Gold. *Discuss. Faraday Soc.* **1951**, *11*, 55–75.
- (65) Sanz-Ortiz, M. N.; Sentosun, K.; Bals, S.; Liz-Marzán, L. M. Templated Growth of Surface Enhanced Raman Scattering-Active Branched Gold Nanoparticles within Radial Mesoporous Silica Shells. *ACS Nano* **2015**, *9*, 10489–10497.
- (66) Li, D.; He, Q.; Li, J. Smart Core/Shell Nanocomposites: Intelligent Polymers Modified Gold Nanoparticles. *Adv. Colloid Interface Sci.* **2009**, *149*, 28–38.
- (67) Luo, C.; Dong, Q.; Qian, M.; Zhang, H. Thermosensitive Polymer-Modified Gold Nanoparticles with Sensitive Fluorescent Properties. *Chem. Phys. Lett.* **2016**, *664*, 89–95.
- (68) Taghizadeh, S.; Alimardani, V.; Roudbali, P. L.; Ghasemi, Y.; Kaviani, E. Gold Nanoparticles Application in Liver Cancer. *Photodiagn. Photodyn. Ther.* **2019**, *25*, 389–400.
- (69) Schaertl, W.; Roos, C. Convection and Thermodiffusion of Colloidal Gold Tracers by Laser Light Scattering. *Phys. Rev. E: Stat. Phys., Plasmas, Fluids, Relat. Interdiscip. Top.* **1999**, *60*, 2020–2028.